Journal of Neural Engineering

PAPER

RECEIVED
4 April 2026

REVISED
7 June 2026

ACCEPTED FOR PUBLICATION
15 June 2026

PUBLISHED
3 July 2026

High-definition transcranial random noise stimulation enhances fluid intelligence with increasing cortical excitability

Tianyi Zheng[1,*], **Yunshan Huang**[1], **Masato Sugino**[1], **Kenta Shimba**[1], **Yasuhiko Jimbo**[2] and **Kiyoshi Kotani**[1]

[1] Department of Human and Engineered Environmental Studies, The University of Tokyo, 277-0882 Chiba, Japan
[2] Department of Precision Engineering, The University of Tokyo, 113-0033 Tokyo, Japan
[*] Author to whom any correspondence should be addressed.

E-mail: zheng@neuron.t.u-tokyo.ac.jp

Keywords: fluid intelligence, reasoning, transcranial random noise stimulation (tRNS), electroencephalography (EEG), reaction time, cortical excitability

Abstract

Objective. Fluid intelligence is a core component of higher-order cognition, yet whether high-definition high-frequency transcranial random noise stimulation (HD/HF-tRNS) can enhance demanding reasoning performance and modulate its neural correlates remains unclear. *Approach.* We investigated the after-effects of offline HD/HF-tRNS targeting the right dorsolateral prefrontal cortex (DLPFC). In a double-blind, sham-controlled, between-groups design, 26 healthy adults completed Raven's progressive matrices (RPM) before and after receiving active or sham stimulation. Electroencephalography (EEG) was recorded during task and resting-state sessions. Behavioral outcomes were accuracy and reaction time; neurophysiological outcomes were high-gamma mean spatial phase synchronization and the aperiodic exponent of neural power spectra. *Main results.* Active HD/HF-tRNS did not significantly alter accuracy but selectively reduced reaction time on the most difficult RPM items. During hard-level trials, reaction time decreased after active stimulation but not after sham stimulation, and post-stimulation reaction time was lower in the active group than in the sham group. High-gamma spatial phase synchronization increased after active stimulation, and the aperiodic exponent decreased during medium- and hard-level trials, with effects predominantly over the right hemisphere. No significant stimulation-related changes were observed during resting state. *Significance.* Offline HD/HF-tRNS over the right DLPFC facilitated response speed during demanding fluid-intelligence performance and induced task-dependent changes in EEG-derived correlates of cortical excitability. These findings support HD/HF-tRNS as a focal neuromodulatory approach for probing neural processes engaged during demanding reasoning.

1. Introduction

Fluid intelligence (g_f) encompasses the ability to reason, solve problems, and think abstractly, independent of acquired knowledge [1]. It is fundamental to a wide range of cognitive tasks and is among the strongest predictors of academic achievement, occupational performance, and cognitive resilience [1]. Raven's progressive matrices (RPM) is the gold standard non-verbal measure of fluid intelligence, engaging analytic reasoning, relational integration, and visuospatial processing across items of graded difficulty [2–4]. Characterizing the neural systems that support RPM performance is therefore an important step toward identifying biologically grounded targets for modulating demanding reasoning processes.

The neural substrates of fluid intelligence have been characterized by the Parieto-Frontal integration theory, which identifies a distributed network spanning the dorsolateral prefrontal cortex (DLPFC; Brodmann areas 9, 46), inferior and superior parietal lobules, anterior cingulate cortex, and temporal–occipital regions [5]. Within this network, the DLPFC plays a pivotal role. Neuroimaging and lesion studies have demonstrated that the DLPFC is heavily involved in working memory maintenance, cognitive flexibility, attentional selection, and abstract reasoning—all core components of fluid intelligence [6–8]. The

right DLPFC merits particular attention as a stimulation target: right-lateralized frontal regions show increased activation when rule complexity increases during abstract reasoning [9], and lesion evidence confirms the right DLPFC's critical role in visuospatial manipulation tasks [10]. Modulation of cortical excitability in the DLPFC has been shown to influence fluid intelligence directly, with studies demonstrating that enhancing neural excitability in this region improves performance on tasks requiring cognitive control and problem-solving [11, 12].

Transcranial random noise stimulation (tRNS) has emerged as a promising neuromodulation technique for increasing cortical excitability. tRNS delivers weak alternating current at random frequencies through scalp electrodes, and high-frequency (HF) tRNS (100–640 Hz) was first shown to increase cortical excitability—as indexed by motor-evoked potential (MEP) amplitudes—by Terney *et al* [13], with after-effects lasting approximately 60 min. The efficacy of tRNS depends on the breadth of the frequency band: only broad-band stimulation (e.g. 100–640 Hz) reliably enhances excitability, whereas narrower sub-ranges alone do not produce significant effects [14]. tRNS also offers practical advantages over transcranial direct current stimulation (tDCS), including no polarity dependence, superior blinding due to reduced cutaneous sensation, and charge-balanced waveforms [15].

Proposed mechanisms of stimulation-induced after-effects differ across transcranial electrical stimulation (tES) waveforms. For tDCS, pharmacological studies combining stimulation with transcranial magnetic stimulation (TMS)-based measures of motor cortical excitability have shown that an N-methyl-D-aspartate (NMDA)-receptor antagonist suppresses post-stimulation effects, while sodium-channel blockade selectively abolishes anodal excitability increases, supporting contributions from both membrane polarization and NMDA-receptor-dependent plasticity [16]. For tRNS, pharmacological evidence instead suggests that the excitability-enhancing after-effects are attenuated by blockade of voltage-gated sodium channels, whereas NMDA-receptor antagonism or partial agonism does not reliably modify the effect under the tested parameters [17]. These findings point to an important contribution of membrane ion-channel dynamics to tRNS after-effects, although its cellular and network-level mechanisms remain incompletely resolved.

At a functional level, stochastic resonance (SR) has been proposed as a complementary account of how random-noise stimulation may facilitate information processing: adding an appropriate amount of noise to a nonlinear system can improve the detection or transmission of weak inputs. Studies applying tRNS to visual cortex reported noise-dependent enhancement of near-threshold perceptual detection consistent with SR [18], and combined behavioral and computational modeling work indicated that tRNS can accelerate evidence accumulation for weak visual signals [19]. Because these observations were obtained in perceptual decision-making tasks rather than in reasoning, SR provides a mechanistic motivation for the present study but is not directly tested by the current design.

High-definition (HD) electrode montages offer further advantages over conventional configurations. Conventional tRNS typically employs large electrodes (e.g. 5×7 cm) that stimulate broad cortical areas, making it difficult to attribute observed effects to specific brain regions. In contrast, HD montages—such as the $4{\times}1$ ring configuration—use a smaller center electrode surrounded by return electrodes, constraining the electric field to the cortical area circumscribed by the return electrodes and achieving substantially greater spatial focality [20, 21]. Importantly, Kuo *et al* [21] demonstrated that HD stimulation produces a more delayed peak effect (at approximately 30 min) and significantly longer-lasting after-effects (exceeding 2 h) compared to conventional montages—a finding that informed the 30 min delay between stimulation offset and post-stimulation testing in the present study. A recent study directly comparing HD-tRNS with conventional tRNS found that the HD montage produced faster learning, greater performance improvements, and superior retention on a complex cognitive task [12]. For these reasons, a HD/HF-tRNS protocol targeting the right DLPFC was employed in the present study.

To characterize the neurophysiological effects of HD/HF-tRNS, the present study employed two electroencephalography (EEG)-based correlates of cortical excitability. The first is the mean spatial phase synchronization (R-value) in the high gamma frequency band (55–95 Hz). Critically, Pellegrino *et al* [22] tested multiple EEG-derived excitability estimates against TMS-measured cortical excitability and found that spatial phase synchrony in the high gamma band covaried positively with MEP amplitudes, supporting its use as an EEG correlate of stimulation-related excitability changes. Related work has confirmed that noise exposure can modulate spatial phase synchronization in a region-specific manner [23]. The second index is the aperiodic exponent (χ-value) derived from the parameterization of the neural power spectrum using the Fitting oscillations & one-over-F (FOOOF) algorithm [24]. The aperiodic exponent reflects the slope of the $1/f$-like background component of the power spectrum and has been linked to excitation–inhibition (E/I) balance: computational modeling has associated a flatter spectrum (smaller exponent) with greater excitatory dominance and a steeper spectrum (larger exponent) with greater inhibitory dominance [25], a relationship supported by empirical evidence across pharmacological, developmental, and cognitive contexts [25, 26]. A decrease in the χ-value can therefore be

interpreted as consistent with a relative shift toward greater excitatory dominance, while remaining an indirect spectral correlate rather than a direct measurement of synaptic E/I balance. Both measures were selected based on prior evidence that they are sensitive to excitability-related changes in the context of brain stimulation [14, 22].

While previous studies have demonstrated that transcranial alternating current stimulation (tACS) [27–30] and tDCS [11] can modulate fluid intelligence, and that tRNS enhances cortical excitability [13, 14], no study to date has combined HD/HF-tRNS with EEG-based excitability correlates to investigate task-related neural changes accompanying fluid-intelligence performance. The present study fills this gap by investigating the after-effects of offline HD/HF-tRNS targeting the right DLPFC on performance in a fluid-intelligence task and cortical excitability in a double-blind, sham-controlled, between-groups design. Twenty-six healthy participants completed RPM before and after receiving either active or sham HD/HF-tRNS, while EEG was recorded during both task and resting-state sessions. We hypothesized that active HD/HF-tRNS would improve RPM performance, particularly under higher task demand, and that this behavioral effect would be accompanied by increased cortical excitability, reflected by increased spatial phase synchronization and a decreased aperiodic exponent.

2. Methods and materials

2.1. Participants

This study was approved by the Research Ethics Committee at The University of Tokyo based on the Research Ethics Review Implementation Rules of The University of Tokyo (23–595). The main trial was conducted according to the guidelines of the Declaration of Helsinki. The participants provided their written informed consent to participate in this study.

Twenty-six healthy volunteers (7 females; age 24.2 ± 2.9 years, mean [M] ± standard deviation [SD]) participated in this study. All participants had normal or corrected-to-normal visual acuity and no history of neurological or psychiatric disorders. Because caffeine, nicotine, and alcohol can influence brain dynamics [31], cognitive function [32], and the effects of tRNS [15], participants were instructed to abstain from these substances for at least 24 hours before the experiment.

2.2. Procedure

Data were collected at The University of Tokyo, Japan. Prior to the experiment, the rationale and potential risks of the study, the potential side effects of tRNS (e.g. slight tingling, burning, heat, and itching sensations over the scalp), and participants' right to withdraw at any time were explained.

As illustrated in figure 1(A), the experiment comprised five sessions: a pre-tRNS task, a pre-tRNS resting state, active or sham tRNS, a post-tRNS resting state, and a post-tRNS task. EEG was recorded during all resting-state and task sessions (see section 2.4). Each task session was preceded by a 30 s baseline resting period during which participants fixated on a central cross on the screen. The RPM test was used to assess fluid intelligence; participants completed one task session before and one after the tRNS intervention, each lasting 10–20 min depending on individual response speed. Long resting-state recordings lasted 3 min each and were acquired once before and once after tRNS. The tRNS intervention lasted 20 min.

A 30 min delay was imposed between tRNS offset and the post-tRNS resting state, based on evidence that the effects of tES on cortical excitability peak approximately 30 min after stimulation offset [14, 21].

Participants completed two questionnaires: one before the experiment to obtain demographic information (age, sex, medical history, ongoing medication) and caffeine, nicotine, and alcohol consumption in the past month; and one after the tRNS session to report any stimulation-induced sensations (itching, pain, burning, heat, metallic taste, fatigue, and general state). Participants were seated in a comfortable chair throughout the experiment. The laboratory was kept quiet and bright during resting state and RPM task sessions.

2.3. RPM test

RPM is a non-verbal test of abstract reasoning widely regarded as a standard measure of fluid intelligence [2–4]. As illustrated in figure 1(B), each item presented a matrix of geometric designs with one piece missing, and the participant was instructed to select the most appropriate completion from multiple options. The present study used all 60 items from Raven's standard progressive matrices and 22 of 48 items from Raven's advanced progressive matrices, yielding 82 items in total. The remaining 26 items were excluded because they were either duplicated items or involved qualitatively different reasoning rules, and because limiting each task session to fewer than 20 min was necessary to minimize mental fatigue.

Participants responded by clicking a numbered box displayed on screen. Visual feedback confirmed each response, but no correctness information was provided. Six practice items with feedback were completed before the first task session to ensure participants understood the procedure. Each participant completed all 82 items: 41 in the pre-tRNS task and 41 in the post-tRNS task. Because item difficulty increases progressively within each RPM set, adjacent items were randomly assigned to the pre- or post-tRNS task for each participant, with a 50%

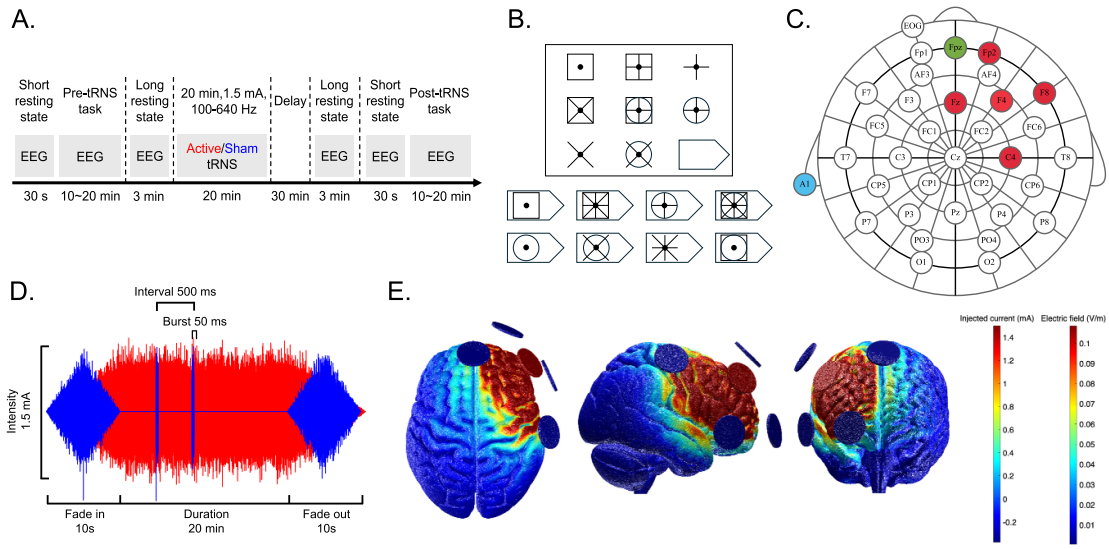

Figure 1. (A) Timeline of the double-blind, sham-controlled experiment. Participants completed a pre-tRNS RPM task (preceded by a 30-s baseline resting period) and a 3 min resting-state EEG, followed by 20 min active or sham HD/HF-tRNS. After a 30 min delay, a 3 min post-tRNS resting-state EEG and a post-tRNS RPM task (preceded by a 30-s baseline resting period) were recorded. (B) Example of a Raven's progressive matrices (RPM) item. Participants selected the option that can best complete the missing element in the matrix from the choices shown below. (C) Electrode configuration based on the international 10–20 system (31 EEG channels and one EOG channel), with A1 (left ear) as the common reference and Fpz as the common ground (green). The corresponding tRNS electrode placement during the active/sham tRNS session is marked as red on the 10-20 system. (D) Stimulation waveforms. Active HD/HF-tRNS delivered Gaussian noise band-pass filtered at 100–640 Hz (peak-to-peak 1.5 mA; 10 s fade-in, 20 min stimulation, 10 s fade-out). Sham stimulation ramped up and down over 10 s and delivered brief noise bursts (50 ms) every 500 ms during the main stage. (E) ROAST-based electric-field simulation (New York head model) for the 4×1 montage targeting right DLPFC (center: F4; peripheral: Fz, F8, Fp2, C4). Maps show superior, right-lateral, and anterior views of the modeled field. Electrode colors indicate injected current (mA), and the cortical color scale indicates electric-field magnitude (V m^{-1}), with warmer colors representing higher magnitudes. The modeled field was concentrated over the right frontal cortex beneath the F4-centered montage, including the targeted right DLPFC.

probability for each assignment. Participants were instructed to prioritize accuracy over speed.

2.4. EEG data acquisition

EEG was recorded during all resting-state and task sessions. The recording system comprised two EEG amplifiers (g.USBamp), two active-electrode driver boxes (g.GAMMAbox), an elastic EEG cap (g.EEGcap), 32 active Ag/AgCl electrodes (31 EEG electrodes and one electrooculography (EOG) electrode; g.ACTIVEelectrode), one ground electrode (g.ACTIVEground, Ag/AgCl), and one reference ear clip (g.GAMMAearclip, Ag/AgCl; all components from g.tec Medical Engineering GmbH, Schiedlberg, Austria). The EOG channel was recorded to identify and remove ocular artifacts. Conductive gel (g.GAMMAgel, g.tec) was applied to all electrodes. Electrodes were positioned according to the international 10–20 system (figure 1(C)), with A1 (left ear) as the common reference and Fpz as the common ground. Trigger signals were sent from the stimulus computer to the EEG amplifier via a microcontroller board (Arduino Uno, arduino.cc) to synchronize task events with the EEG recording. Data were digitized at 4800 Hz with an online band-pass filter of 0.01–500 Hz and a notch filter at 50 Hz (48–52 Hz) to suppress power-line interference. EEG data were acquired using MATLAB Simulink [33].

2.5. HD/HF-tRNS

A previous study demonstrated that offline HD tDCS delivered with a 4×1 ring montage (center: F4; peripheral: Fz, F8, Fp2, and C4 of the international 10–20 system [34]) reduced reaction times on RPM [11]. The present study adopted the same electrode placement for HD/HF-tRNS to target the DLPFC, a region critical for fluid intelligence [8, 35].

Prior to stimulation, skin preparation gel (skinPure, NIHON KOHDEN, Tokyo, Japan) was applied to the targeted scalp areas to reduce impedance. HD/HF-tRNS was delivered by a battery-driven current stimulator (nurostym tES^{TM}, Neuro Device Group S.A., Warsaw, Poland) through rubber carbon electrodes (Amrex CM-A102; 3 × 3 cm) affixed with conductive paste (Ten20, Weaver and Company, Aurora, CO), tape, and supporting bandage. Impedance was maintained below 10 kΩ throughout stimulation, as monitored in real time by the stimulator. As illustrated in figure 1(D), active HD/HF-tRNS consisted of Gaussian noise band-pass filtered at 100–640 Hz with a peak-to-peak amplitude of 1.5 mA (i.e. 99% of the injected current intensity fell below this value), delivered for 20 min with 10 s fade-in and fade-out periods. Sham stimulation ramped up to 1.5 mA and back to 0 over 10 s at both the beginning and end, with brief noise bursts (100–640 Hz, peak-to-peak 1.5 mA) delivered every 500 ms

Table 1. Contingency table of conditioning and reporting stimulation group.

	Report active	Report sham
Condition active	4	9
Condition sham	5	8

Group differences in reported stimulation condition were evaluated using Fisher's exact test ($p = 1.00$).

during the main stage to mimic scalp sensations without sustained cortical stimulation.

The study employed a double-blind, sham-controlled design to control for placebo effects [36, 37]. Participants were randomly assigned to either the sham ($N = 13$) or active ($N = 13$) stimulation group and were unaware of their group assignment. Blinding success was assessed by asking participants to guess their stimulation condition at the end of the tRNS session. As shown in table 1, participants could not distinguish active from sham stimulation at better than chance level (Fisher's exact test, $p = 1.00$). Stimulation was well tolerated, with only mild and transient side effects reported (e.g. itching and pain near the electrodes, phosphene perception).

To characterize the spatial distribution of the stimulation, we simulated the electric field of HD/HF-tRNS using the realistic volumetric-approach to simulate transcranial electric stimulation (ROAST) package [38, 39] with the New York Head magnetic resonance imaging template [40]. The simulation confirmed that the induced electric field predominantly affected the right DLPFC region (figure 1(E)).

2.6. Data analysis and statistics

2.6.1. Behavior data

Statistical analysis of behavioral data were conducted in Python using NumPy [41], pandas [42], SciPy [43], and statsmodels [44]. Only reaction times from correct trials were analyzed. Trials were categorized into three difficulty levels (easy, medium, and hard) based on mean reaction time in the pre-tRNS task averaged across both groups (see section 3.1 for details). A three-way repeated-measures analysis of variance (ANOVA) was performed on reaction time data with two within-participant factors—task time (pre-/post-tRNS) and difficulty level (easy, medium, hard)—and one between-participant factor—group (sham/active) [45–47]. Post hoc pairwise comparisons were conducted using *t*-tests with Bonferroni correction [48] to examine differences in reaction time between pre- and post-tRNS conditions and between sham and active groups.

2.6.2. EEG preprocessing

EEG preprocessing and analysis were performed in Python using MNE-Python [49], NumPy [41], pandas [42], and SciPy [43]. A high-pass filter at 0.3 Hz was applied to remove slow drifts. Notch filters at 100, 150, 200, and 250 Hz were applied to remove residual power-line harmonics (the fundamental 50 Hz harmonic was already removed online during acquisition). Bad channels (1.6 ± 1.1 per participant, $M \pm SD$) were identified by visual inspection of waveforms and power spectra. Ocular artifacts were attenuated using the signal-space projection method with one projection vector [50]. The EEG was then re-referenced to the average of all non-bad channels, and bad channels were reconstructed using spherical spline interpolation [51]. After interpolation, all 31 EEG channels were retained for every participant and included in subsequent EEG analysis; the EOG channel was used only for ocular-artifact correction and was excluded from these analysis.

Continuous EEG data were epoched by trial, from stimulus onset (question appearance) to either the participant's response or the onset of the next question. For the final trial of each task session, the epoch extended from stimulus onset to either the response or 90 s post-onset.

2.6.3. Mean spatial phase synchronization

Mean spatial phase synchronization (*R*-value) was used as an EEG-based correlate of cortical excitability [22, 52, 53]. Positive correlations between *R*-value and cortical excitability have been reported in previous studies [22, 52]. For this measure, each epoched EEG segment was band-pass filtered in the high-gamma range (55–95 Hz), selected based on prior work evaluating spatial phase synchrony as an excitability correlate [22, 23]. Filtering was implemented in MNE-Python (version 1.8.0) using a zero-phase finite impulse response (FIR) filter with a Hamming window and the `firwin` design. The filter used reflective signal padding at segment boundaries (`pad = reflect_limited`) to reduce filter-edge artifacts; for the 55–95 Hz band at the 4800-Hz sampling rate, the FIR filter length was 1153 samples (0.240 s). The resulting measure was interpreted as a predefined band-limited high-gamma synchrony index, rather than as the phase of a single narrow-band oscillation. The analytic signal of the band-pass-filtered data $X_k(t)$ was then obtained using a Hilbert transform $H[X_k(t)]$, and the phase trace of each channel $\theta_k(t)$ was computed as

$$\theta_k(t) = \arctan \frac{H[X_k(t)]}{X_k(t)}, \tag{1}$$

where k denotes the channel number, which is 1–31 in the current study. Next, the Kuramoto order parameter $r(t)$ was computed as [54]:

$$r(t) = \frac{1}{N} \left| \sum_{k=1}^{N} e^{i\theta_k(t)} \right|, \tag{2}$$

where i is the imaginary unit. Finally, mean spatial phase synchronization, referred to here as the R-value, was quantified by

$$R\text{-value} = \langle r(t) \rangle = \frac{1}{L} \sum_{t=1}^{L} r(t), \tag{3}$$

where t denotes the time point and L is the number of time points in the data segment. For statistical analysis, a two-way repeated-measures ANOVA was performed with task time (pre-/post-tRNS) as a within-participant factor and group (sham/active) as a between-participant factor. Post hoc pairwise comparisons were conducted using t-tests with Bonferroni correction [48].

To examine the frequency specificity of the high-gamma R-value findings, follow-up analysis additionally computed R-values separately in four adjacent sub-bands (55–65, 65–75, 75–85, and 85–95 Hz). Within each task-difficulty condition and resting state, participant-level change scores (ΔR-value = post-tRNS minus pre-tRNS) were compared between the active and sham groups using two-sided permutation tests, and Hedges' g was calculated as an effect-size estimate. To examine whether the task-related high-gamma R-value effects depended on ongoing high-gamma activity before stimulation, we conducted an exploratory baseline-state analysis. Mean 55–95 Hz power was computed from each participant's pre-tRNS resting-state segment across the 31 EEG channels using multitaper power spectral density estimation; values were $\log_{10}$ transformed and standardized across participants. For medium- and hard-level trials, broad-band ΔR-values were entered into separate linear models with group, baseline high-gamma power, and their interaction as predictors. The group × baseline-power interaction was evaluated using two-sided randomization tests with 100 000 group-label permutations. To control for multiple comparisons in the frequency-specific follow-up analysis, raw p values from the 16 predefined active-versus-sham comparisons (four high-gamma sub-bands × three task-difficulty conditions and resting state) were adjusted using the Benjamini–Hochberg false discovery rate (FDR) procedure. Results are reported with FDR-adjusted p values after uncorrected permutation-test, with $p < .05$ considered statistically significant.

2.6.4. Phase-amplitude coupling

To examine whether HD/HF-tRNS enhanced cross-frequency coupling related to the task-dependent high-gamma findings, we conducted targeted exploratory phase-amplitude coupling (PAC) analysis. For the primary PAC analysis, delta phase (1–4 Hz) was selected based on prior reports relating delta–gamma coupling to fluid-intelligence performance [55], and lower high-gamma amplitude (55–65 Hz) was selected based on the sub-band R-value findings in the present study. Two predefined sensitivity analysis evaluated delta-phase coupling to the original broad high-gamma amplitude band (55–95 Hz) and alpha-phase (8–12 Hz) coupling to broad high-gamma amplitude (55–95 Hz), the latter addressing a commonly studied alpha–gamma PAC relationship. Continuous task EEG recordings were resampled to 600 Hz and band-pass filtered before task-trial samples were extracted, thereby avoiding filter boundaries at individual trial edges. PAC was quantified using the Tort modulation index with 18 phase bins [56], computed separately for each of the 31 EEG channels and averaged within each participant and session. The analysis included correct medium- and hard-level trials lasting at least 4 s. Within each difficulty level, the same number of pooled time samples was used for each participant and session before calculating each PAC measure. Participant-level PAC change scores (post-tRNS minus pre-tRNS) were compared between active and sham groups using two-sided permutation tests.

2.6.5. Aperiodic exponent estimation (FOOOF)

The aperiodic exponent was estimated using the FOOOF algorithm, which parameterizes each neural power spectrum into an aperiodic 1/f-like background plus periodic (oscillatory) peaks [24]. For each dataset entry, we analyzed 31 EEG channels (ch 1–31) and computed power spectral densities (PSDs) using the multitaper method with discrete prolate spheroidal sequence tapers implemented in MNE-Python [49], with sampling frequency $sfreq = 4800$ Hz and PSD range 1–100 Hz. FOOOF was then fit independently for each channel over the fitting range 3–40 Hz. Following the FOOOF documentation, frequencies and PSD values were provided in linear scale (FOOOF internally fits in $\log_{10}$(power) space) [24]. We used the default FOOOF settings (`peak_width_limits` = (0.5, 12) Hz, `max_n_peaks` = ∞, `min_peak_height` = 0, `peak_threshold` = 2.0, `aperiodic_mode` = `fixed`). The neural power spectrum was parameterized using the FOOOF method, which represents the spectrum as the sum of an aperiodic background component and a set of Gaussian peaks corresponding to oscillatory activity [24]:

$$\mathrm{PSD}(F) = L(F) + \sum_{n=0}^{N} G_n(F), \tag{4}$$

$$G_n(F) = a_n \exp\left(\frac{-(F-c_n)^2}{2\omega_n^2}\right), \tag{5}$$

$$L(F) = b - \log(k + F^X), \tag{6}$$

where F denotes frequency, N is the number of detected spectral peaks, and $G_n(F)$ is the Gaussian function used to describe the nth oscillatory peak. For each peak, a_n indicates the peak power in $\log_{10}$ units,

c_n is the center frequency, and ω_n is the SD of the Gaussian. The aperiodic component $L(F)$ is described by the offset b, the exponent χ, and the knee parameter k, which allows curvature in the aperiodic spectrum. When $k = 0$, the model reduces to a linear aperiodic component in log–log space. In the present study, the aperiodic exponent χ was used as the spectral index of cortical excitability, motivated by prior work linking the spectral exponent to cortical state and E/I balance [25, 26]. In the FOOOF output, this value was obtained from `aperiodic_params` as the exponent term [24].

To assess statistical significance while controlling for multiple comparisons across electrodes, we used a cluster-based permutation test with spatial adjacency among EEG sensors. Sensor adjacency was constructed from standard 10–20 electrode coordinates by computing the inter-electrode distance matrix yielding a binary adjacency matrix. For each difficulty level, four comparisons were tested: (1) sham pre vs. post, (2) active pre vs. post, (3) pre sham vs. active, and (4) post sham vs. active. We applied `permutation_cluster_1samp_test` for within-subjects comparison and `permutation_cluster_test` for between-subjects comparison with 2000 permutations using the adjacency matrix. The test returns an F-statistic at each electrode, and we converted it to a signed t-value by $t = \sqrt{F} \cdot \text{sign}(t)$, where the sign was determined from the direction of the channel-wise difference between the two conditions. Clusters were considered significant at $p < .05$, and the signed test statistics were visualized as scalp topographies.

3. Results

3.1. Preliminary analysis of task performance

Behavioral performance was assessed by two measures: accuracy (proportion of correct responses) and reaction time (time from stimulus onset to mouse click). Because reaction time is meaningful only for correct responses, accuracy was analyzed first.

As summarized in table 2, four participants in the sham group and three in the active group showed decreased accuracy from pre- to post-tRNS, while three sham and one active participant showed unchanged accuracy. The remaining participants (six sham, nine active) showed improved accuracy. Although more participants in the active group showed improvement, this difference was not statistically significant (Fisher's exact test on improved vs. not improved, $p = .43$).

Reaction times from correct trials were then analyzed. Questions were classified into three difficulty levels based on the mean reaction time in the pre-tRNS task (averaged across both groups): easy-level (<10 s; 27 questions), medium-level (10–20 s; 27 questions), and hard-level (⩾20 s; 28 questions).

Table 2. Accuracy changes from pre- to post-tRNS in the active and sham groups.

	Active group	Sham group
Lower accuracy	3	4
Equal accuracy	1	3
Higher accuracy	9	6

Group differences in the proportion of participants with higher accuracy versus those with equal or lower accuracy were evaluated using Fisher's exact test ($p = .43$).

3.2. Reaction time reduction in hard-level trials after active HD/HF-tRNS

Reaction times for correct trials were submitted to a 2 (group) × 2 (task time) × 3 (difficulty level) repeated-measures ANOVA. The omnibus analysis revealed significant main effects of group ($F(1,24) = 6.62$, $p = .02$, $\eta_p^2 = .216$), task time ($F(1,24) = 5.01$, $p = .03$, $\eta_p^2 = 0.173$), and difficulty level ($F(2,48) = 4.96$, $p < .01$, $\eta_p^2 = 0.171$). The two-way interaction of group × difficulty level was significant ($F(1,24) = 3.98$, $p = .03$, $\eta_p^2 = 0.142$), whereas neither the group × task time ($F(2,48) = 0.49$, $p = .62$, $\eta_p^2 = 0.020$) nor the task time × difficulty level ($F(2,48) = 0.22$, $p = .80$, $\eta_p^2 < 0.001$) interactions reached significance. The three-way interaction of group × task time × difficulty level was significant ($F(2,48) = 3.36$, $p = .04$, $\eta_p^2 = 0.123$). Given the large effect size for difficulty level, follow-up analysis were conducted separately for each difficulty level.

For easy-level trials, a 2 × 2 repeated-measures ANOVA revealed significant main effects of group ($F(1,24) = 4.53$, $p = .04$, $\eta_p^2 = 0.159$) and task time ($F(1,24) = 5.14$, $p = .03$, $\eta_p^2 = 0.177$), but the group × task time interaction was not significant ($F(1,24) = 0.95$, $p = .34$, $\eta_p^2 = 0.038$). Post hoc pairwise comparisons (figure 2(A)) confirmed significant reaction time reductions in both the sham group ($p < .01$; from 6.3 s to 5.5 s) and the active group ($p < .01$; from 6.4 s to 5.1 s). No significant differences were observed between groups at either pre-tRNS ($p = .86$) or post-tRNS ($p = .75$).

For medium-level trials, there was a significant main effect of task time ($F(1,24) = 9.80$, $p < .01$, $\eta_p^2 = 0.290$) but not of group ($F(1,24) = 0.04$, $p = .84$, $\eta_p^2 = 0.002$). The group × task time interaction did not reach significance ($F(1,24) = 3.54$, $p = .07$, $\eta_p^2 = 0.129$). Post hoc comparisons (figure 2(B)) showed that the reaction time reduction was not significant in the sham group ($p = .59$; from 13.3 s to 12.7 s) but was significant in the active group ($p = .02$; from 13.1 s to 11.4 s). No significant between-group differences were observed at either time point (pre: $p = .43$; post: $p = .30$).

For hard-level trials, significant main effects were observed for both group ($F(1,24) = 7.25$, $p = .01$, $\eta_p^2 = 0.232$) and task time ($F(1,24) = 6.23$, $p = .02$, $\eta_p^2 = 0.206$), and the group × task time interaction was also significant ($F(1,24) = 4.71$, $p = .04$, $\eta_p^2 =$

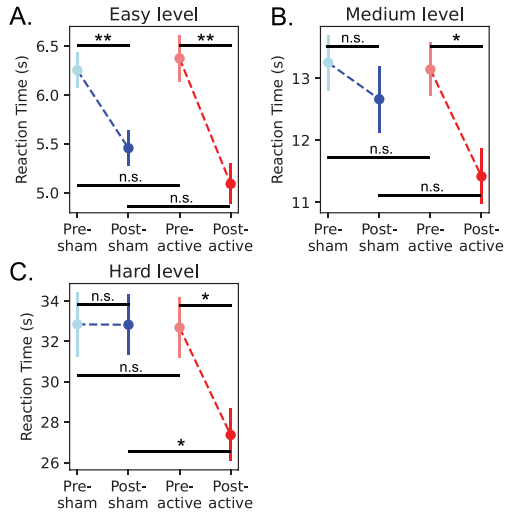

Figure 2. Reaction time changes from pre-tRNS to post-tRNS for (A) easy-level, (B) medium-level, and (C) hard-level trials. Light blue and blue dots represent mean reaction times for the sham group (pre- and post-tRNS, respectively); light red and red dots represent mean reaction times for the active group (pre- and post-tRNS, respectively). Vertical lines indicate 95% confidence intervals, and horizontal lines identify the conditions included in each pairwise comparison. Pairwise comparisons were conducted using *t*-tests with Bonferroni correction ($*p < .05$, $**p < .01$, n.s., not significant). In (A), reaction time decreased significantly in both groups, with no significant between-group differences. In (B), reaction time decreased significantly only within the active group, while between-group differences were not significant. In (C), reaction time decreased significantly only within the active group, and post-tRNS reaction time was significantly lower in the active group than in the sham group.

0.164). Post hoc comparisons (figure 2(C)) showed that the sham group exhibited no significant reaction time change ($p = .96$; from 32.8 s to 32.8 s), whereas the active group showed a significant reduction ($p = .03$; from 32.7 s to 27.4 s). Pre-tRNS reaction times did not differ between groups ($p = .77$), but post-tRNS reaction times were significantly lower in the active than in the sham group ($p = .03$). Thus, the stimulation-specific effect of offline HD/HF-tRNS on reaction time—beyond general practice effects—was significant only for hard-level RPM items.

3.3. HD/HF-tRNS enhanced spatial phase synchronization in high-gamma frequency bands

To examine EEG correlates of the after-effects of HD/HF-tRNS on cortical excitability, two measures were computed from epoched data of correct trials, classified by difficulty level: mean spatial phase synchronization in the high gamma band (*R*-value) and the aperiodic exponent (χ-value) from the FOOOF algorithm.

For easy-level trials, no significant main effects of group ($F(1,24) = 1.31$, $p = .26$, $\eta_p^2 = 0.052$) or task time ($F(1,24) = 1.29$, $p = .27$, $\eta_p^2 = 0.051$) were observed, and the group × task time interaction was not significant ($F(1,24) = 0.45$, $p = .51$, $\eta_p^2 = 0.018$). Post hoc comparisons (figure 3(A)) revealed no significant pairwise differences (all $p > .05$).

For medium-level trials, a 2 × 2 repeated-measures ANOVA on *R*-values revealed no significant main effects of group ($F(1,24) = 1.95$, $p = .28$, $\eta_p^2 = 0.049$) or task time ($F(1,24) = 2.86$, $p = .10$, $\eta_p^2 = 0.107$), but a significant group × task time interaction ($F(1,24) = 12.74$, $p < .01$, $\eta_p^2 = 0.347$). Post hoc comparisons (figure 3(B)) showed that *R*-value increased significantly after active tRNS ($p < .01$), but was not significantly higher in the post-active than the post-sham condition ($p > .05$; all other pairwise comparisons $p > .05$).

For hard-level trials, the main effect of task time was significant ($F(1,24) = 6.97$, $p = .01$, $\eta_p^2 = 0.225$), but not of group ($F(1,24) = 0.57$, $p = .46$, $\eta_p^2 = 0.023$). The group × task time interaction was significant ($F(1,24) = 5.25$, $p = .03$, $\eta_p^2 = 0.180$). Post hoc comparisons (figure 3(C)) showed that the *R*-value increase from pre- to post-active was significant ($p = .02$) and was significantly higher in the post-active than the post-sham condition ($p = .03$; all other pairwise comparisons $p > .05$).

To assess whether stimulation effects extended beyond the task state, *R*-values during resting state were also examined. The 2 × 2 repeated-measures ANOVA revealed no significant main effects of group ($F(1,24) = 3.15$, $p = .09$, $\eta_p^2 = 0.116$) or task time ($F(1,24) = 0.02$, $p = .89$, $\eta_p^2 < 0.001$), and no significant interaction ($F(1,24) = 0.28$, $p = .60$, $\eta_p^2 < 0.012$). Post hoc comparisons (figure 3(D)) confirmed no significant pairwise differences (all $p > .05$).

Follow-up analysis in narrower high-gamma sub-bands further examined the frequency specificity of the *R*-value effect (figures 3(E)–(H)). In the 55–65 Hz sub-band, the active-versus-sham difference in ΔR-value was significant during medium-level trials (difference = 0.0442, Hedges' $g = 0.740$, $p = .03$) and during hard-level trials (difference = 0.0471, Hedges' $g = 0.789$, $p = .02$). The stimulation-related *R*-value increase during the more demanding task conditions was pronounced in the lower high-gamma range.

Finally, an exploratory baseline-state analysis examined whether pre-tRNS resting-state high-gamma power moderated the broad-band *R*-value changes during the task conditions in which stimulation-related changes were observed. The group × baseline-power interaction was not significant for either medium-level trials ($\beta = -0.0032$, randomization $p = .91$) or hard-level trials ($\beta = 0.0067$, randomization $p = .82$). Thus, within the present sample, there was no evidence that the task-related *R*-value changes depended on individual differences in baseline ongoing high-gamma power.

Targeted exploratory PAC analysis also did not identify significant stimulation-related enhancement. In the primary analysis of delta-phase to 55–65 Hz amplitude PAC, the active-versus-sham difference in PAC change was not significant during medium-level

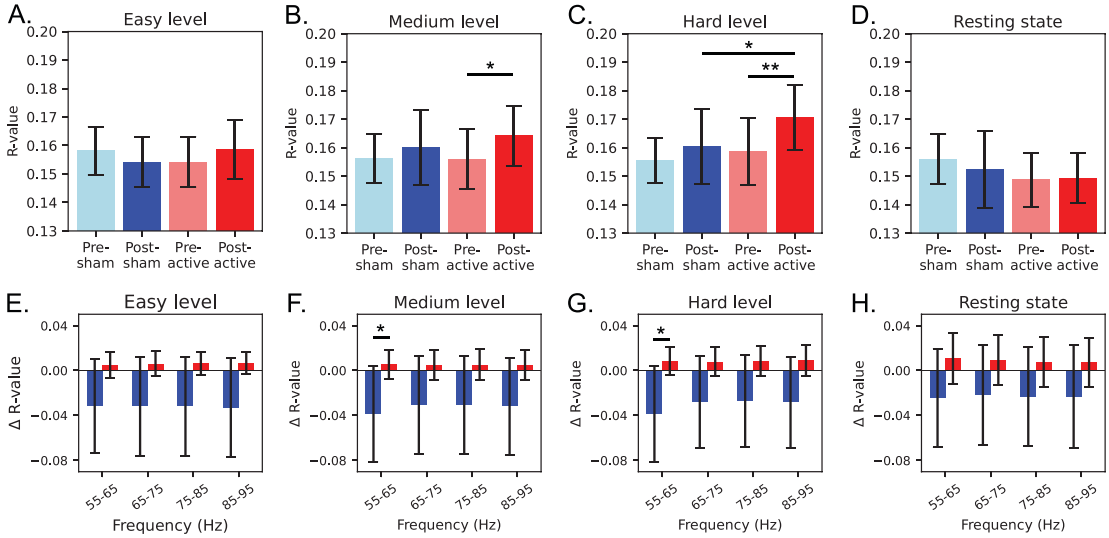

Figure 3. Mean spatial phase synchronization (R-value) in the broad high-gamma band (55–95 Hz) for (A) easy-level, (B) medium-level, and (C) hard-level trials, and (D) resting state. Follow-up frequency-specific analysis of the pre-to-post change in R-value (ΔR-value) are shown for (E) easy-level, (F) medium-level, and (G) hard-level trials, and (H) resting state across four high-gamma sub-bands. In panels A–D, light blue and blue bars represent the sham group (pre- and post-tRNS, respectively), and light red and red bars represent the active group (pre- and post-tRNS, respectively). Horizontal lines and asterisks indicate significant Bonferroni-corrected pairwise t-tests: no pairwise differences were significant in (A) or (D); R-value increased after active stimulation in (B) and (C); and the post-tRNS active-group R-value exceeded that of the sham group in (C). In panels E–H, blue and red bars represent ΔR-value in the sham and active groups, respectively. Error bars denote 95% confidence intervals. Asterisks in panels E–H indicate significant active-versus-sham differences in ΔR-value ($^*p < .05$, FDR-adjusted two-sided permutation test): the 55–65 Hz band was significant in (F) and (G), and no sub-band difference was significant in (H).

trials (difference = 0.000 257, Hedges' $g = 0.461$, $p = .27$) or hard-level trials (difference = −0.000 023, Hedges' $g = -0.039$, $p = .95$). Sensitivity analysis using the broad 55–95 Hz amplitude band similarly showed no significant active-versus-sham difference for delta-phase PAC (medium: difference = 0.000 282, Hedges' $g = 0.521$, $p = .18$; hard: difference = −0.000 027, Hedges' $g = -0.041$, $p = .95$) or alpha-phase PAC (medium: difference = 0.000 005, Hedges' $g = 0.039$, $p = .94$; hard: difference = 0.000 024, Hedges' $g = 0.229$, $p = .58$). Thus, the present results did not provide evidence that the high-gamma R-value effects were accompanied by enhanced cross-frequency coupling in these predefined PAC measures.

In summary, in the broad 55–95 Hz high-gamma band, active HD/HF-tRNS enhanced spatial phase synchronization (R-values) during medium- and hard-level tasks, with no observable effects during easy-level trials or the resting state. Notably, such increase observed during hard-level trials was strictly tRNS-specific, as it was significantly greater than in the sham condition. Follow-up sub-band analysis further identified significant active-versus-sham changes at 55–65 Hz during both medium- and hard-level trials.

3.4. Decreased aperiodic exponent after active HD/HF-tRNS

For easy-level trials, cluster-based permutation analysis of the aperiodic exponent (χ-value) revealed no significant clusters across any comparison (figure 4(A)).

For medium-level trials, significant clusters were observed in which χ-value decreased over the frontal and right temporal region (pre-active vs. post-active, $p = .01$) and over the right frontal, parietal, and temporal region (post-sham vs. post-active, $p < .01$; figure 4(B). No significant clusters were found for the pre-sham vs. pre-active or pre-sham vs. post-sham comparisons.

For hard-level trials, significant clusters were observed in which χ-value decreased over the right temporal and occipital region (pre-active vs. post-active, $p = .04$) and over the right temporal region (post-sham vs. post-active, $p = .04$; figure 4(C). No significant clusters were found for the pre-sham vs. pre-active or pre-sham vs. post-sham comparisons.

For resting state, no significant clusters were observed across any comparison (figure 4(D)).

In summary, the aperiodic exponent was significantly decreased after active HD/HF-tRNS during medium-level and hard-level task trials, with significant clusters predominantly over the right hemisphere, but not during easy-level trials or resting state.

4. Discussion

The present study investigated the after-effects of offline HD/HF-tRNS targeting the right DLPFC on performance in a fluid-intelligence task and

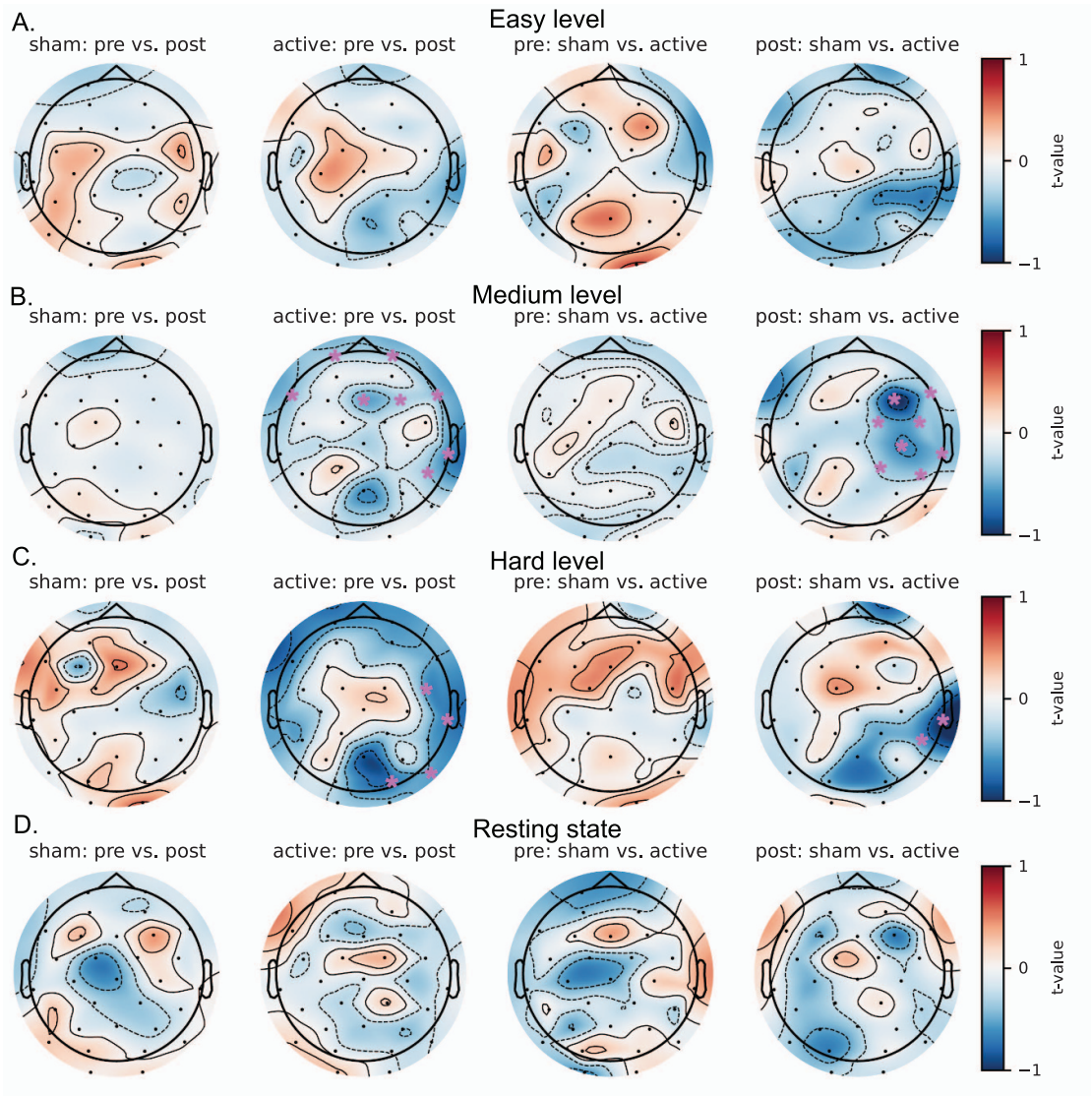

Figure 4. Topographic maps of aperiodic exponent (χ-value) changes for (A) easy-level, (B) medium-level, and (C) hard-level trials, and (D) resting state. Scalp maps are viewed from above with the nose at the top; the left side of each map represents the left hemisphere. Within each row, maps display (left to right): sham pre vs. post, active pre vs. post, pre sham vs. active, and post sham vs. active comparisons. Color scale represents *t*-values from cluster-based permutation tests; positive values (red) indicate that the latter condition has a higher χ-value, whereas negative values (blue) indicate that the latter condition has a lower χ-value. Violet stars mark electrodes forming significant clusters (cluster-level permutation $p < .05$). No significant clusters occurred in (A) or (D). In (B), significant decreases after active stimulation were distributed over frontal and right temporal regions, and significantly lower post-tRNS values in the active group than in the sham group were distributed over right frontal, parietal, and temporal regions. In (C), significant decreases after active stimulation were distributed over right temporal and occipital regions, and significantly lower post-tRNS values in the active group than in the sham group were distributed over the right temporal region.

cortical excitability. Three main findings emerged: (1) the stimulation-specific effect of HD/HF-tRNS on reaction time—beyond general practice effects observed in both groups—was significant only for hard-level RPM questions; (2) spatial phase synchronization in the high gamma band (*R*-value) was significantly increased after active stimulation during medium-level and hard-level trials; and (3) the aperiodic exponent (χ-value) was significantly decreased after active stimulation during medium-level and hard-level trials, with significant clusters predominantly over the right hemisphere. Together, these behavioral and neurophysiological results are consistent with HD/HF-tRNS facilitating demanding reasoning performance while altering EEG correlates of task-related cortical excitability.

4.1. After-effects of HD/HF-tRNS on behavioral performance in the RPM Task

No statistically significant difference was observed in accuracy between groups, reflecting ceiling performance in healthy young adults, which is consistent with prior studies that similarly found reaction time as the primary outcome of brain stimulation on RPM [11, 28, 29]. Analysis of reaction times revealed a difficulty-dependent pattern of enhancement. Both groups showed significant reaction time reductions for easy-level questions (a general practice effect),

with no significant group × task time interaction. For medium-level questions, the active group showed a significant reduction whereas the sham group did not, though the interaction did not reach statistical significance. Critically, for hard-level questions, only the active group showed a significant reduction, the group × task time interaction was significant, and the reaction time in the post-active task was significantly lower than in the post-sham task. This difficulty-dependent pattern—where the stimulation-specific effect emerges most clearly on the most demanding reasoning questions—is a robust finding in the brain stimulation literature on fluid intelligence, having been demonstrated in after-effect studies using gamma tACS [28, 29] and theta tACS [30].

The SR framework offers one possible account of this difficulty-selectivity. Under this hypothesis, random-noise input may be most beneficial when task-relevant processing is weak or near threshold; harder RPM items could therefore be more amenable to facilitation than easy items [18, 19]. Additionally, harder RPM items require greater engagement of the right DLPFC for maintaining and manipulating multiple relational representations simultaneously [10], making performance on these items potentially more sensitive to excitability changes in the stimulated region. However, RPM difficulty is not a direct measure of neural signal threshold, and the present study did not test whether baseline behavioral performance predicted stimulation-related reaction-time changes. The behavioral pattern is therefore compatible with, but does not establish, an SR mechanism; it supports a selective improvement in response speed under high task demand rather than a generalized enhancement of fluid intelligence per se.

4.2. Task-dependent EEG correlates of cortical excitability following offline HD/HF-tRNS

The present neurophysiological findings should be interpreted in the context of evidence concerning the after-effects of HF-tRNS. In motor cortex, HF-tRNS increases TMS-evoked excitability for a period after stimulation [13, 14], and pharmacological evidence indicates sensitivity of these after-effects to sodium-channel blockade rather than a necessary contribution of NMDA receptors under the tested stimulation conditions [17]. This literature provides a plausible basis for altered cortical responsivity following offline HD/HF-tRNS, but the current EEG data do not measure ion-channel activity or synaptic plasticity directly. Rather, they characterize task-evoked cortical dynamics recorded after stimulation in the context of demanding reasoning.

The first EEG finding was increased *R*-value, a measure of spatial phase synchrony in the high-gamma range, during medium- and hard-level trials. Pellegrino *et al* [22] reported that high-gamma spatial phase synchrony covaried positively with TMS-derived cortical excitability, and related work found that noise exposure can alter this measure in a region-specific manner [23]. In the present data, follow-up analysis further localized the medium- and hard-level changes to the lower portion of the predefined high-gamma range (55–65 Hz). Gamma-band synchronization is associated with coordinated interactions between excitatory pyramidal neurons and inhibitory interneurons [57]; accordingly, increased *R*-value is compatible with more coordinated recruitment of task-engaged populations after stimulation. However, because HF-tRNS delivers broadband random noise rather than periodic stimulation, the result should not be interpreted as evidence that stimulation entrained an endogenous gamma rhythm or established a specific cellular mechanism.

The second EEG finding was a decrease in the aperiodic exponent during medium- and hard-level trials, with significant clusters predominantly over the right hemisphere. The aperiodic exponent characterizes the broadband, non-oscillatory component of the neural spectrum. Computational and empirical work has linked a flatter exponent to a relative shift toward excitatory dominance in population-level E/I balance [25, 26], and recent work has related aperiodic activity to corticospinal excitability [58]. The decrease observed here is therefore consistent with increased excitability of task-recruited cortical populations. At the same time, the exponent remains an indirect spectral marker rather than a direct measurement of synaptic excitation and inhibition. The convergence of a lower exponent and higher high-gamma synchrony during the same higher-demand task conditions is consequently best viewed as converging EEG evidence for altered task-related excitability, rather than proof that one neural process caused the other.

The condition specificity of the results offers a functional interpretation of these after-effects. Behavioral improvement was clearest for hard-level trials, while the primary broadband *R*-value and aperiodic-exponent findings occurred during medium- and hard-level performance but not during easy-level trials or rest. Overall, the higher-demand pattern is compatible with activity-selective modulation of engaged circuits [59] and with the stochastic-resonance (SR) account, under which added noise is most beneficial for near-threshold processing [18, 19]. Nonetheless, the present study did not manipulate noise intensity or task-signal threshold and therefore cannot directly establish SR as the mediating mechanism. Similarly, exploratory analysis did not show that baseline resting-state high-gamma power moderated the *R*-value changes, and predefined PAC analysis did not show enhanced delta- or alpha-phase coupling to high-gamma amplitude. These null findings constrain the interpretation: the observed after-effects are compatible with enhanced task-related cortical responsivity, but are not evidence for baseline-state dependency or increased cross-frequency coupling. Larger studies

with experimental manipulations directed at these candidate mechanisms will be necessary to distinguish among them.

4.3. Comparison with prior brain stimulation studies of fluid intelligence

The present findings can be situated within the broader brain stimulation literature targeting fluid intelligence. The results converge with Arif *et al* [11] in several respects: both studies used HD stimulation (4×1 montage) targeting the right DLPFC, and both found reaction time improvements as the primary behavioral outcome. However, Arif *et al* found decreased alpha/beta parieto-frontal connectivity following HD-tDCS, which they interpreted as reflecting more efficient neural processing, while the present study found increased gamma phase synchronization and aperiodic exponent changes following HD/HF-tRNS—reflecting the different mechanisms of tRNS versus tDCS.

A particularly notable comparison is with Santarnecchi *et al* [29], who targeted left middle frontal gyrus and found that conventional (non-HD) tRNS at 101–640 Hz did not produce the same frequency-specific enhancement of fluid intelligence as 40 Hz gamma tACS. In contrast, the present study demonstrates that HD/HF-tRNS targeting the right DLPFC selectively improves response speed on difficult RPM items, suggesting that the improved spatial focality of HD montages can be important for obtaining measurable behavioral effects with tRNS. This interpretation aligns with the findings of Chenot *et al* [12] that HD-tRNS outperformed conventional tRNS on complex cognitive tasks. Whereas gamma-frequency tACS is designed to apply a periodic input at a defined frequency, HD/HF-tRNS delivers broadband random input. The present findings are therefore compatible with altered cortical responsivity that supports high-gamma synchronization during reasoning, rather than demonstrating direct entrainment of gamma oscillations.

4.4. Limitations and future directions

The sample size ($N = 26$, with 13 per group), while within the range typical for tES studies [15], is modest and limits statistical power to detect smaller effects. Although participants were randomly assigned to stimulation groups, the primary analysis did not adjust for demographic or baseline individual-difference variables, including age, sex, pre-stimulation RPM performance, or baseline neurophysiological characteristics such as resting-state aperiodic exponent. In a small between-groups sample size, residual imbalance in such characteristics could influence estimated effects and restrict generalization to broader populations. Recent work has demonstrated that baseline aperiodic exponent predicts tRNS response [60], suggesting that individual E/I balance is an important potential moderator of stimulation efficacy. Although our targeted exploratory analysis found no evidence that pre-stimulation resting-state high-gamma power moderated the *R*-value after-effect, this analysis does not constitute a comprehensive covariate or moderator assessment. Future research should prioritize larger-sample, multi-session designs with pre-specified adjustment analysis to determine whether HD/HF-tRNS produces cumulative benefits on fluid intelligence and to evaluate individual differences in response. Calibrating stimulation intensity to individual baseline E/I balance represents a promising direction for optimizing HD/HF-tRNS protocols [60].

The post-stimulation assessment was initiated approximately 30 min after HD/HF-tRNS offset, at a time selected to capture previously reported delayed excitability after-effects. Because no additional follow-up assessments were obtained, the present study cannot determine the duration of the observed behavioral or EEG after-effects. Future studies with multiple post-stimulation time points are needed to characterize their temporal persistence.

Finally, the scalp EEG measures used in the present study are affected by volume conduction and therefore cannot provide precise intracranial source localization; consequently, the observed right-lateralized scalp distributions should not be interpreted as direct localization of their cortical generators. Future studies could combine HD/HF-tRNS with source-resolved neuroimaging approaches. In particular, ultrasound-modulated EEG and acoustoelectric brain imaging have been proposed to combine the temporal resolution of electrophysiological signals with the spatial focusing provided by transcranial ultrasound, and recent proof-of-concept studies have demonstrated high-precision localization and waveform decoding of intracranial dipole sources in simulation and experimental platforms [61, 62]. Further validation and application of these approaches in human brain-stimulation studies may enable more precise characterization of intracranial cortical dynamics following HD/HF-tRNS.

The present study included a template-based ROAST finite-element simulation to characterize the nominal spatial distribution of the induced electric field over the right DLPFC (figure 1(E)). Future studies could extend this approach using subject-specific anatomical models and electrode-placement estimates to quantify individual differences in field magnitude and orientation at the target and test whether these modeled dose measures predict behavioral and EEG after-effects [38, 40]. A complementary mechanistic approach would use field-informed biophysical network or spiking-neuron models in which broadband stochastic input is scaled according to the modeled local field. Such models could test whether plausible stimulation levels increase coordinated high-gamma activity and flatten

aperiodic spectra in task-engaged E/I networks, and whether any simulated benefit is greatest for near-threshold or high-demand reasoning process, as predicted by stochastic-resonance accounts [19, 25]. Relating these simulations to the observed 55–65 Hz synchronization effect, the null PAC enhancement, and behavioral difficulty selectivity would help distinguish spatial-dose, stochastic-resonance, and circuit-excitability explanations of the current findings.

5. Conclusions

The present study provides the first evidence that HD/HF-tRNS targeting the right DLPFC can modulate performance on a demanding fluid-intelligence task together with EEG-derived markers of cortical excitability during active cognitive engagement. Active HD/HF-tRNS selectively reduced reaction times on hard-level RPM questions, whereas accuracy was not significantly altered. Two EEG-based measures-spatial phase synchronization in the high gamma band (R-value) and the aperiodic exponent (χ-value)-showed changes consistent with increased task-related cortical excitability after active stimulation, but not at rest. These findings support HD/HF-tRNS as a useful tool for probing neural processes engaged during demanding reasoning performance and motivate further work to determine whether repeated or larger-scale interventions can produce broader gains in fluid intelligence.

Acknowledgment

This research is partially supported by Japan Society for the Promotion of Science through a Grant-in-Aid for DC1 Fellows (KAKENHI), Grant No. 22J22909, to T Z, the Precise Measurement Technology Promotion Foundation, the Asahi Glass Foundation, and The Canon Foundation to K K.

Data availability statement

The data cannot be made publicly available upon publication because they contain sensitive personal information. The data that support the findings of this study are available upon reasonable request from the authors.

Author contributions

Tianyi Zheng 0009-0002-8250-4071
Conceptualization (lead), Data curation (equal), Formal analysis (lead), Funding acquisition (equal), Investigation (lead), Methodology (lead), Project administration (equal), Software (lead), Visualization (lead), Writing – original draft (lead)

Yunshan Huang 0009-0000-1627-0011
Formal analysis (equal), Investigation (equal), Methodology (equal), Visualization (equal)

Masato Sugino 0009-0009-1309-2331
Data curation (lead), Methodology (equal), Resources (equal), Software (equal)

Kenta Shimba 0000-0003-1156-260X
Data curation (equal), Project administration (equal), Supervision (equal), Writing – review & editing (equal)

Yasuhiko Jimbo 0009-0004-6005-5043
Data curation (equal), Project administration (equal), Resources (equal), Supervision (equal), Writing – review & editing (equal)

Kiyoshi Kotani
Conceptualization (equal), Data curation (equal), Funding acquisition (lead), Investigation (equal), Project administration (lead), Resources (equal), Supervision (lead), Writing – review & editing (lead)

References

[1] Shipstead Z, Harrison T L and Engle R W 2016 Working memory capacity and fluid intelligence: Maintenance and disengagement *Perspect. Psychol. Sci.* **11** 771–99
[2] Raven J C 1936 Mental tests used in genetic studies: the performance of related individuals on tests mainly educative and mainly reproductive *MSC Thesis* (University of London)
[3] Raven J C 1941 Standardization of progressive matrices, 1938 *Br. J. Med. Psychol.* **19** 137–50
[4] Raven J C, Court J H, Forbes A R and Foulds G A 1958 *Advanced Progressive Matrices* (H K Lewis & Company)
[5] Jung R E and Haier R J 2007 The Parieto-Frontal Integration Theory (P-FIT) of intelligence: converging neuroimaging evidence *Behav. Brain Sci.* **30** 135–54
[6] Cieslik E C *et al* 2013 Is There "One" DLPFC in cognitive action control? evidence for heterogeneity from co-activation-based parcellation *Cereb. Cortex* **23** 2677–89
[7] Friedman N P and Robbins T W 2022 The role of prefrontal cortex in cognitive control and executive function *Neuropsychopharmacology* **47** 72–89
[8] Nikolaidis A, Baniqued P L, Kranz M B, Scavuzzo C J, Barbey A K, Kramer A F and Larsen R J 2017 Multivariate Associations of Fluid Intelligence and NAA *Cereb. Cortex* **27** 2607–16
[9] Hampshire A, Thompson R, Duncan J and Owen A M 2011 Lateral prefrontal cortex subregions make dissociable contributions during fluid reasoning *Cereb. Cortex* **21** 1–10
[10] Barbey A K, Colom R and Grafman J 2013 Dorsolateral prefrontal contributions to human intelligence *Neuropsychologia* **51** 1361–9
[11] Arif Y, Spooner R K, Heinrichs-Graham E and Wilson T W 2021 High-definition transcranial direct current stimulation modulates performance and alpha/beta parieto-frontal connectivity serving fluid intelligence *J. Physiol.* **599** 5451–63
[12] Chenot Q, Hamery C, Lepron E, Besson P, De Boissezon X, Perrey S and Scannella S 2022 Performance after training in a complex cognitive task is enhanced by high-definition transcranial random noise stimulation *Sci. Rep.* **12** 4618
[13] Terney D, Chaieb L, Moliadze V, Antal A and Paulus W 2008 Increasing human brain excitability by transcranial

high-frequency random noise stimulation *J. Neurosci.* **28** 14147–55
[14] Moret B, Donato R, Nucci M, Cona G and Campana G 2019 Transcranial random noise stimulation (trns): a wide range of frequencies is needed for increasing cortical excitability *Sci. Rep.* **9** 15150
[15] Antal A *et al* 2017 Low intensity transcranial electric stimulation: safety, ethical, legal regulatory and application guidelines *Clin. Neurophysiol.* **128** 1774–809
[16] Liebetanz D, Nitsche M A, Tergau F and Paulus W 2002 Pharmacological approach to the mechanisms of transcranial DC-stimulation-induced after-effects of human motor cortex excitability *Brain* **125** 2238–47
[17] Chaieb L, Antal A and Paulus W 2015 Transcranial random noise stimulation-induced plasticity is NMDA-receptor independent but sodium-channel blocker and benzodiazepine sensitive *Front. Neurosci.* **9** 125
[18] van der Groen O and Wenderoth N 2016 Transcranial random noise stimulation of visual cortex: stochastic resonance enhances central mechanisms of perception *J. Neurosci.* **36** 5289–98
[19] van der Groen O, Tang M F, Wenderoth N, Mattingley J B and Beck J 2018 Stochastic resonance enhances the rate of evidence accumulation during combined brain stimulation and perceptual decision-making *PLoS Comput. Biol.* **14** e1006301
[20] Capizzi M, Visalli A, Wiener M and Mioni G 2023 The contribution of the supplementary motor area to explicit and implicit timing: a high-definition transcranial random noise stimulation (HD-TRNS) study *Behav. Brain Res.* **445** 114383
[21] Kuo H-I, Bikson M, Datta A, Minhas P, Paulus W, Kuo M-F and Nitsche M A 2013 Comparing cortical plasticity induced by conventional and high-definition 4×1 ring tdcs: a neurophysiological study *Brain Stimul.* **6** 644–8
[22] Pellegrino G, Schuler A-L, Cai Z, Marinazzo D, Tecchio F, Ricci L, Tombini M, Di Lazzaro V and Assenza G 2024 Assessing cortical excitability with electroencephalography: a pilot study with EEG-ITBS *Brain Stimul.* **17** 176–83
[23] Schuler A-L, Brkić D, Ferrazzi G, Arcara G, Marinazzo D and Pellegrino G 2023 Auditory white noise exposure results in intrinsic cortical excitability changes *iScience* **26** 107387
[24] Donoghue T *et al* 2020 Parameterizing neural power spectra into periodic and aperiodic components *Nat. Neurosci.* **23** 1655–65
[25] Gao R, Peterson E J and Voytek B 2017 Inferring synaptic excitation/inhibition balance from field potentials *NeuroImage* **158** 70–78
[26] Waschke L, Donoghue T, Fiedler L, Smith S, Garrett D D, Voytek B and Obleser J 2021 Modality-specific tracking of attention and sensory statistics in the human electrophysiological spectral exponent *eLife* **10** e70068
[27] Klink K, Paßmann S, Kasten F H and Peter J 2020 The modulation of cognitive performance with transcranial alternating current stimulation: a systematic review of frequency-specific effects *Brain Sci.* **10** 932
[28] Santarnecchi E, Polizzotto N R, Godone M, Giovannelli F, Feurra M, Matzen L, Rossi A and Rossi S 2013 Frequency-dependent enhancement of fluid intelligence induced by transcranial oscillatory potentials *Curr. Biol.* **23** 1449–53
[29] Santarnecchi E, Muller T, Rossi S, Sarkar A, Polizzotto N R, Rossi A and Kadosh R C 2016 Individual differences and specificity of prefrontal gamma frequency-tacs on fluid intelligence capabilities *Cortex* **75** 33–43
[30] Neubauer A C, Wammerl M, Benedek M, Jauk E and Jaušovec N 2017 The influence of transcranial alternating current stimulation (tacs) on fluid intelligence: an FMRI study *Pers., Individ. Differ.* **118** 50–55
[31] Vergara V M, Weiland B J, Hutchison K E and Calhoun V D 2018 The impact of combinations of alcohol, nicotine and cannabis on dynamic brain connectivity *Neuropsychopharmacology* **43** 877–90
[32] Lorist M and Snel J 1998 *Nicotine, Caffeine and Social Drinking: Behaviour and Brain Function* 1st edn (Routledge)
[33] The MathWorks Inc 2020 (Natick, MA: The MathWorks Inc) Simulink: Simulation and Model-Based Design
[34] Homan R W, Herman J and Purdy P 1987 Cerebral location of international 10–20 system electrode placement *Electroencephalogr. Clin. Neurophysiol.* **66** 376–82
[35] Arabaci G, Cakir B S and Parris B A 2024 The effect of high-frequency rtms over left dlpfc and fluid abilities on goal neglect *Brain Struct. Funct.* **229** 1073–86
[36] Romanella S M *et al* 2023 Targeting neural correlates of placebo effects *Cogn. Affect. Behav. Neurosci.* **23** 217–36
[37] Braga M, Barbiani D, Andani M E, Villa-Sánchez B, Tinazzi M and Fiorio M 2021 The role of expectation and beliefs on the effects of non-invasive brain stimulation *Brain Sci.* **11** 1526
[38] Huang Y, Datta A, Bikson M and Parra L C 2019 Realistic volumetric-approach to simulate transcranial electric stimulation – roast – a fully automated open-source pipeline *J. Neural Eng.* **16** 056006
[39] Huang Y, Datta A, Bikson M and Parra L C 2018 ROAST: an open-source, fully-automated, Realistic vOlumetric-Approach-based Simulator for TES *Annu. Int. Conf. IEEE Eng. Med. Biol. Soc.* (*Honolulu, Jul 2018*) (https://doi.org/10.1109/EMBC.2018.8513086)
[40] Huang Y, Parra L C and Haufe S 2016 The new york head - a precise standardized volume conductor model for eeg source localization and tes targeting *NeuroImage* **140** 150–62
[41] Harris C R *et al* 2020 Array programming with NumPy *Nature* **585** 357–62
[42] McKinney W *et al* 2010 Data structures for statistical computing in python *Proc. 9th Python in Science Conf.* pp 51–56
[43] Virtanen P *et al* SciPy 1.0 Contributors 2020 SciPy 1.0: fundamental algorithms for scientific computing in Python *Nat. Methods* **17** 261–72
[44] Seabold S and Perktold J 2010 Statsmodels: Econometric and statistical modeling with python *9th Python in Science Conf.* 92–96
[45] Mashal N and Metzuyanim-Gorelick S 2019 New information on the effects of transcranial direct current stimulation on n-back task performance *Exp. Brain Res.* **237** 1315–24
[46] Du X-D *et al* 2022 Delayed improvements in visual memory task performance among chronic schizophrenia patients after high-frequency repetitive transcranial magnetic stimulation *World J. Psychiatry* **12** 1169–82
[47] Imbert L, Moirand R, Bediou B, Koenig O, Chesnoy G, Fakra E and Brunelin J 2022 A single session of bifrontal tdcs can improve facial emotion recognition in major depressive disorder: an exploratory pilot study *Biomedicines* **10** 2397
[48] Armstrong R A 2014 When to use the bonferroni correction *Ophthal. Physiol. Opt.* **34** 502–8
[49] Gramfort A *et al* 2013 MEG and EEG data analysis with MNE-Python *Front. Neurosci.* **7** 1–13
[50] Uusitalo M A and Ilmoniemi R J 1997 Signal-space projection method for separating meg or eeg into components *Med. Biol. Eng. Comput.* **35** 135–40
[51] Perrin F, Pernier J, Bertrand O and Echallier J F 1989 Spherical splines for scalp potential and current density mapping *Electroencephalogr. Clin. Neurophysiol.* **72** 184–7
[52] Meisel C, Schulze-Bonhage A, Freestone D, Cook M J, Achermann P and Plenz D 2015 Intrinsic excitability measures track antiepileptic drug action and uncover increasing/decreasing excitability over the wake/sleep cycle *Proc. Natl Acad. Sci.* **112** 14694–9
[53] Meisel C, Plenz D, Schulze-Bonhage A and Reichmann H 2016 Quantifying antiepileptic drug effects using intrinsic excitability measures *Epilepsia* **57** e210–5
[54] Kuramoto Y 1975 Self-entrainment of a population of coupled non-linear oscillators *Int. Symp. on Mathematical*

Problems in Theoretical Physics vol 39, ed H Araki (Springer) pp 420–2

[55] Gagol A, Magnuski M, Kroczek B, Kałamała P, Ociepka M, Santarnecchi E and Chuderski A 2018 Delta-gamma coupling as a potential neurophysiological mechanism of fluid intelligence *Intelligence* **66** 54–63

[56] Tort A B L, Komorowski R, Eichenbaum H and Kopell N 2010 Measuring phase-amplitude coupling between neuronal oscillations of different frequencies *J. Neurophysiol.* **104** 1195–210

[57] Buzsáki G and Wang X-J 2012 Mechanisms of gamma oscillations *Annu. Rev. Neurosci.* **35** 203–25

[58] Jin J, Wang X, Zhao X, Wang H, Li Y, Liu Z and Yin T 2025 Aperiodic brain activity modulates corticospinal excitability *Neurosci. Bull.* (https://doi.org/10.1007/s12264-025-01559-1)

[59] Bikson M and Rahman A 2013 Origins of specificity during tDCS: anatomical, activity-selective and input-bias mechanisms *Front. Hum. Neurosci.* **7** 688

[60] van Bueren N E R, van der Ven S H G, Hochman S, Sella F and Kadosh R C 2023 The role of cortical excitation-inhibition balance in tRNS efficacy *PLoS Biol.* **21** e3002193

[61] Zhang H, Zhang Y, Wang X, Chen G, Jian X, Xu M and Ming D 2023 Transcranial dipole localization and decoding study based on ultrasonic phased array for acoustoelectric brain imaging *J. Neural Eng.* **20** 066001

[62] Zhang H, Wang X, Chen G, Zhang Y, Jian X, He F, Xu M and Ming D 2025 Noninvasive intracranial source signal localization and decoding with high spatiotemporal resolution *Cyborg Bionic Syst.* **6** 0206